

Modeling and Control of a Hybrid Electric Vehicle With an Electrically Assisted Turbocharger

Achin Jain, Tobias Nueesch, Christian Naegele, Pedro Macri Lassus, and Christopher H. Onder

Abstract—This paper investigates the suitability of using an electrically assisted turbocharger in a hybrid electric vehicle (HEV) with a turbocharged engine, based on fuel economy and acceleration performance. This system has two electric machines, i.e., a traction motor and a boost motor coupled to the shaft of the turbocharger, and offers an additional control variable in the energy management problem i.e., the amount of electrical boost (e-boost) to reduce the turbolag. The task of an optimal controller now becomes manifold: deciding the torque split between the engine and the traction motor, the power of the boost motor, and the gear number. A quasi-static model of a parallel HEV with a turbocharged engine is derived, and a method to model turbolag based on a predefined map for the permissible engine torque is proposed. Dynamic programming (DP) is used to solve the optimal control problem. To find out an optimal tradeoff between the two onboard electric machines, the optimal strategy is calculated with a constraint on the maximum total electrical power. The circumstances in which it is advantageous to use the boost motor are discussed. Furthermore, the influence of powertrain components' size on the control strategy is analyzed, specifically in the problem of maximizing acceleration performance, by scaling the engine displacement volume for different sizes of turbochargers keeping the maximum engine torque and power constant, and scaling the motor map for different nominal power values. The robustness of this modeling approach has also been verified.

Index Terms—Dynamic programming (DP), electrically assisted turbocharger, energy management, hybrid electric vehicle (HEV), optimal control, turbolag.

I. INTRODUCTION

FUELS based on fossils are unquestionably the best on-board energy sources in automobiles, in terms of energy density and refueling time [1]. However, their use is not sustainable and is one of the reasons for growing environmental

Manuscript received April 17, 2015; revised September 1, 2015 and December 17, 2015; accepted February 8, 2016. Date of publication February 23, 2016; date of current version June 16, 2016. The review of this paper was coordinated by Dr. S. Anwar.

A. Jain is with the Real-Time and Embedded Systems Laboratory, University of Pennsylvania, Philadelphia, PA 19104 USA (e-mail: achinj@seas.upenn.edu).

T. Nueesch was with the Institute for Dynamic Systems and Controls, Swiss Federal Institute of Technology in Zurich (ETH Zurich), 8092 Zurich, Switzerland. He is now with ThyssenKrupp Presta AG, 9492 Eschen, Liechtenstein (e-mail: tobias.nueesch@idsc.mavt.ethz.ch).

C. Naegele is with Daimler AG, 70546 Stuttgart, Germany, and also with Brandenburg University of Technology Cottbus-Senftenberg, 03046 Cottbus, Germany (e-mail: christian.naegele@daimler.com).

P. Macri Lassus is with Daimler AG, 70546 Stuttgart, Germany (e-mail: pedro.macri-lassus@daimler.com).

C. H. Onder is with the Institute for Dynamic Systems and Controls, Swiss Federal Institute of Technology in Zurich (ETH Zurich), 8092 Zurich, Switzerland (e-mail: onder@idsc.mavt.ethz.ch).

Color versions of one or more of the figures in this paper are available online at <http://ieeexplore.ieee.org>.

Digital Object Identifier 10.1109/TVT.2016.2533585

concerns. This poses two prime challenges in a conventional vehicle propelled with hydrocarbon-based fuels: improving the fuel economy and reducing the emissions. Many solutions have been used in the past to improve the fuel efficiency, including turbocharging and hybridization. In addition, driveability is another important measure of performance, which assesses vehicle's speed and acceleration characteristics. It also quantifies driving comfort in the form of frequency of engine on-offs, frequency of gear shifts, etc. While the passenger vehicles should be able to meet the basic acceleration demands in a driving cycle with minimal fuel requirements and sometimes also operate in sportive mode, acceleration performance finds more importance over fuel consumption in racing sports. The most common way to improve the driving performance of a turbocharged engine is by means of an electrical assist, which ensures both extra power and high acceleration [2].

A. Turbocharging and Turbocompounding

In a conventional vehicle, without exhaust heat recovery, 30%–40% of energy is lost in the exhaust gas [3]. A turbocharger helps to boost the pressure of the air entering the engine by deriving energy from the exhaust gas, which is otherwise wasted. It allows the engine to be downsized; thus, a turbocharged engine performs more efficiently, reducing fuel consumption and emissions. In a classical turbocharger, a waste gate is used at high engine speeds to regulate the excess boost pressure by limiting the amount of the exhaust gas through the turbine. Clearly, when the waste gate is open, some potential power in the exhaust gas is lost. A variable-geometry turbocharger (VGT) overcomes this drawback by changing the turbine geometry such that the turbocharger can be used in a wide range of engine speeds. The performance of this system, with respect to fuel economy and emissions, can be further improved with turbocompounding.

Several variants of turbocompounding have been proposed in a conventional vehicle [4]. On the basis of topology, turbocompounding may be categorized into two types: 1) electric turbocompounding (ETC) and 2) mechanical turbocompounding (MTC). ETC has proven to be fuel efficient and less emissive in heavy-duty engines, whereas the technology is still immature in small-displacement engines. As much as 10% reduction in fuel consumption is possible with ETC in heavy-duty diesel engines, depending upon the driving cycles [5]–[8]. In addition, ETC can be more effective over its mechanical counterpart because it can exploit the advantage of operating at more efficient points, whereas this is a restriction in the mechanical case because of the coupling with the crankshaft [8], [9]. Turbocompounding

has also shown an adverse effect in small-displacement engines because of high back pressures in the exhaust [10], [11]. However, onboard energy management strategies can provide a further scope of improvement [12].

ETC also improves the response time of the turbocharger. Both designs of the turbocharger (with and without VGT) suffer from an inherent disadvantage of turbolag, which depends on the inertia and efficiency of the turbocharger. A bigger turbocharger has a relatively slower response due to high inertia and low efficiency at small mass flows but can provide high maximum power. Turbocharger with a VGT and same inertia shows less turbolag because of higher efficiency for a wide range of mass flows. The performance in a VGT can be optimized with respect to this characteristic [13]. Electric machine used in ETC when accelerated helps to alleviate the turbolag, i.e., an advantage over both classical turbocharging and MTC [14]–[16].

Thus, turbocompounding is an attractive technology for an efficient propulsion, in terms of both fuel consumption and acceleration response. In particular, ETC can be more efficient and can provide more freedom in defining control strategies in hybrid electric vehicles (HEVs) over its mechanical counterpart, as the new control input (amount of electrical boost) can be controlled independently, while there exists mechanical coupling constraint in MTC [9].

B. Hybridization

With the availability of another onboard energy source, hybridization can potentially decrease both the fuel consumption and the emissions. HEVs can operate at more efficient engine set points, and the engine can be downsized while fulfilling the same maximum power requirements [1]. Other benefits in HEVs come from recuperation as well as energy management between the two power sources. The energy management strategy (EMS) or the so-called supervisory control strategy forms the heart of an HEV design. The EMS can be classified into two groups, i.e., rule-based control strategies/heuristic EMS and numerical optimization-based control strategies, which can be applied offline or online. A comprehensive review of EMS in HEVs can be found in [17]. The role of EMS is to decide the optimal power split between the internal combustion engine and the electric source(s) to reduce the fuel consumption or/and improve the driving performance while satisfying the power demands of the vehicle. In the presence of an electric boost (e-boost) mechanism, EMS must also decide on the amount of e-boost, i.e., the power from the additional motor in ETC.

In early studies, theoretical benefits of ETC with a turbocharged HEV were estimated [4], [18], [19]. Through scaling of data from independent technologies, such as electrical power assist, turbocharging, and hybrid electric powertrains, it has been shown that the assisted turbocharging in light hybrids can achieve the same benefits as in full hybrids [19]. The control strategies for optimizing the performance of e-boost in HEVs has not advanced either. For example, a heuristics-based boost control has been used in [20]. The equivalent consumption minimization strategy (ECMS) has been employed to control the turbocharged HEV in [21]; however, the e-boost is not con-

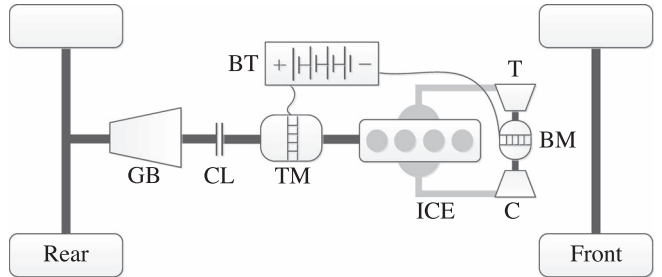


Fig. 1. Topology of a torque-assist HEV.

trolled independently. In [22], optimal control has been applied to maximize the acceleration performance of a conventional turbocharged engine with ETC. This methodology is closely linked to the optimal EMS in HEVs. This serves as a motivation to explore the benefits of the two technologies combined together, i.e., optimal control of HEVs with e-boost. In a more recent study, ETC with a combined hybrid has been analyzed in detail using fuzzy logic and ECMS [23]. A live example of this technology is seen in the 2014 Formula One season [24].

C. Contribution

From the aforementioned literature review, potential benefits of an e-boost in a conventional vehicle are evident in fuel consumption and acceleration performance. However, the energy management in HEVs with an additional electric motor for the boost control needs more investigation. Except for [23], none of the references presents a complete description of the system presented in this paper (see Fig. 1), from both the modeling and control points of view. Zhao *et al.* [23] used online ECMS with a mean value model (MVM) to optimize the fuel consumption in a combined HEV, but the other objective of optimizing the acceleration performance is not addressed at all. Kang *et al.* [25] dealt with the acceleration but only in the context of power-split hybrid. Thus, there exists a need to obtain simple modeling tools, and a systematic approach to deal with this problem, which can also be used for benchmarking. This paper is an attempt in this direction. In particular, we have dealt with the problems of fuel economy and acceleration performance separately. The paper primarily addresses the possibility of improving the performance of a turbocharged HEV by appending an e-boost mechanism, which can reduce the turbolag by the boosting.

This paper is organized as follows. In Section II, the control-oriented model of a “torque-assist” hybrid with a turbocharged engine is derived. A simple approach to model the turbolag and the e-boost mechanism is proposed. Section III discusses the framework to solve the optimal control problem and optimize the control strategy for two different objectives, viz., minimizing the fuel consumption and maximizing the acceleration performance. Section IV presents the simulation conditions and the optimization results for these performance measures. In Section V, the effects of powertrain components’ size on the optimal strategy are analyzed. The robustness of the modeling approach is verified in Section VI. Finally, the paper is concluded with a discussion on the achieved results.

II. HYBRID ELECTRIC VEHICLE MODEL

The vehicle under consideration, i.e., a torque-assist hybrid, is shown in Fig. 1. The vehicle is propelled at the rear wheels. The traction motor (TM) and the internal combustion engine (ICE) are connected to the drivetrain shaft through a torque coupler, which can be decoupled from the drivetrain by using the clutch (CL). The boost motor (BM) is coupled to the turbocharger shaft, which accelerates the compressor (C) and the turbine (T) as commanded by the control strategy. Both motors are connected to the battery (BT). TM is a reversible electric machine, which can also be used to recuperate energy, whereas BM can reduce turbolag by accelerating the turbocharger using energy from BT. The vehicle is incapable of a pure electric drive. The quasi-static models or the backward models described in the following sections have been adapted from [1] and the parameters of this reference model from Mercedes-Benz E-Class.

A. Vehicle Dynamics

The traction force F_t required to drive the vehicle can be expressed as

$$F_t = (m_v + m_r)a + \frac{1}{2}\rho_{\text{air}}A_f C_d v^2 + m_v C_r g \cos(\alpha) + m_v g \sin(\alpha) \quad (1)$$

where m_v is the mass of the vehicle, including that of the engine, the motors, the battery, and the gear box; v is the velocity of the vehicle; and a is the acceleration of the vehicle. ρ_{air} is the density of the air, A_f is the frontal area of the car, and C_d is the aerodynamic drag coefficient. C_r is the rolling friction coefficient, g is the acceleration due to gravity, and α is the slope of the driving path. The rotational mass m_r is a function of the gear ratio γ , the moment of inertia of wheels Θ_w and of the engine Θ_e , and the radius of the wheels r_w , as follows:

$$m_r = \frac{1}{r_w^2} \Theta_w + \frac{\gamma^2}{r_w^2} \Theta_e. \quad (2)$$

Equation (1) can be used to calculate the torque demand at wheels T_w as follows:

$$T_w = F_t r_w. \quad (3)$$

The rotation speed of the wheels is given by

$$\omega_w = \frac{v}{r_w}. \quad (4)$$

B. Gearbox

The vehicle under consideration has seven forward gears. The rotational speed of the drivetrain shaft on the engine side of the gearbox ω_{gb} is related to ω_w as

$$\omega_{\text{gb}} = \gamma \omega_w. \quad (5)$$

The torque on the engine side of the gearbox T_{gb} can be expressed as

$$T_{\text{gb}} = \frac{T_w}{\gamma} \eta_{\text{gb}}^{-\text{sgn}(T_w)} \quad (6)$$

where T_w is negative under recuperation and positive under traction. sgn is the signum function. The corresponding gear number n_g is decided by the control strategy. The gearbox is assumed to have a constant mechanical efficiency.

C. Torque Coupler and Clutch

The electric machine TM is coupled to the drivetrain with direct transmission. Thus, the traction motor and the engine rotate at the same speed. The engine speed ω_e and traction motor speed ω_m can be expressed in terms of ω_{gb} as

$$\omega_e = \omega_m = \begin{cases} \omega_{\text{gb}}, & \text{if clutch is not slipping} \\ \max(\omega_{e,\text{idle}}, \omega_{\text{gb}}), & \text{if clutch is slipping.} \end{cases} \quad (7)$$

The energy balance across the coupler gives a relation between the torque produced by the traction motor T_m and the engine torque T_e , i.e.,

$$T_{\text{gb}} = T_m + T_e \quad (8)$$

$$T_m = \zeta T_{\text{gb}}. \quad (9)$$

The torque split ζ is decided by the control strategy. It lies between $\zeta_{\min} = -1$ and $\zeta_{\max} = 1$. If the battery is sufficiently charged, then the generator might not be able to recuperate the entire energy. Under these conditions, the extra energy is dissipated in friction brakes. It is assumed that there are no energy losses in both the torque coupler and the clutch.

D. Electric Motor/Generator

The reference electric motor/generator (TM) has a maximum power rating of 20 kW. The motor torque is known from (8) and (9). The power P_m as a function of the motor speed ω_m and the motor torque T_m can be calculated from the power map Λ as follows:

$$P_m = \Lambda(\omega_m, T_m). \quad (10)$$

TM works in motor mode when $T_m \geq 0$ and in generator mode when $T_m < 0$. The maximum motor and generator torque $T_{m,\max}$ and $T_{m,\min}$, respectively, depend on the motor speed

$$T_{m,\min}(\omega_m) \leq T_m(\omega_m) \leq T_{m,\max}(\omega_m). \quad (11)$$

E. Internal Combustion Engine

The reference turbocharged gasoline engine has a power rating of 155 kW and can provide a maximum torque of 350 N · m. The fuel consumption of ICE is calculated using a map based on the measurements at stationary operating conditions as a function of the mean effective pressure p_{me} and the engine speed ω_e , i.e.,

$$\dot{m}_f = \Gamma(\omega_e, p_{\text{me}}). \quad (12)$$

The mean effective pressure is related to the engine torque by the expression

$$p_{\text{me}} = \frac{N\pi T_e}{V_d} \quad (13)$$

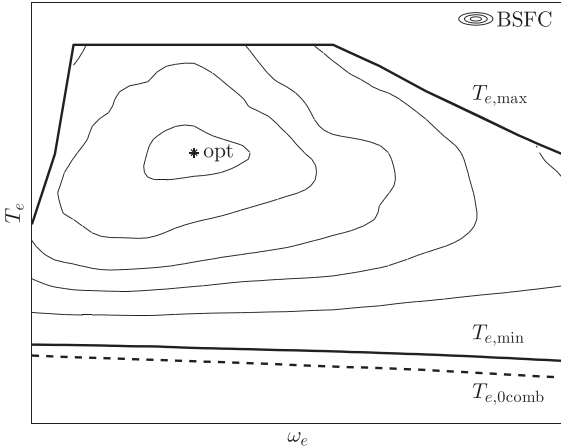


Fig. 2. Torque and efficiency map of the turbocharged gasoline engine under consideration.

where $N = 4$ is used for a four-stroke engine, and V_d is the displacement volume of the engine. The map for brake-specific fuel consumption (BSFC) along with the engine torque at full-load operation or the maximum engine torque $T_{e,\max}$ is shown in Fig. 2. $T_{e,\min}$ is the drag torque, which accounts for all the mechanical losses, and $T_{e,0\text{comb}}$ is the drag torque when combustion is off. Switching between $T_{e,\min}$ and $T_{e,0\text{comb}}$ is discrete.

For the purpose of controls in HEVs, the mean value modeling of the engine is not necessary and the use of stationary maps like Fig. 2 suffices. However, to study the effects of the turbolag and the boost motor in a turbocharged engine, the model must be more complex. In particular, it should also depend on variables, such as inlet air pressure and temperature, exhaust air pressure and temperature, turbocharger speed, and so on. The MVM is one approach to deal with this [26]. The highly complex model in this study considers each engine component and has 13 states. Even if the MVM is simplified, as in [27], where the number of states is seven, the model is dependent on an engine temperature rise map and a volumetric efficiency map, in addition to the turbocharger maps, which are not easily available. The problem size is further reduced by getting rid of the variables with slow dynamics in [28]. Nevertheless, the approach with MVM is not trivial and can also be time consuming. We propose an alternate and a simpler way to model the turbolag behavior. This control-oriented model is also easily adaptable to the e-boost mechanism, which is discussed in the later part of this section.

F. Turbocharger

Many reasonable assumptions have been made while modeling the turbocharger. For instance, throttle, intercooler, intake manifold, exhaust manifold, and exhaust gas regeneration have not been modeled. Of all, the key assumptions are listed as follows.

- A1: Combustion is always carried out at stoichiometric air fuel ratio.
- A2: The pressure and the temperature at the outlet port of the compressor ($p_{c,\text{out}}$, $\vartheta_{c,\text{out}}$) are the same as those in the intake manifold (p_{im} , ϑ_{im}).

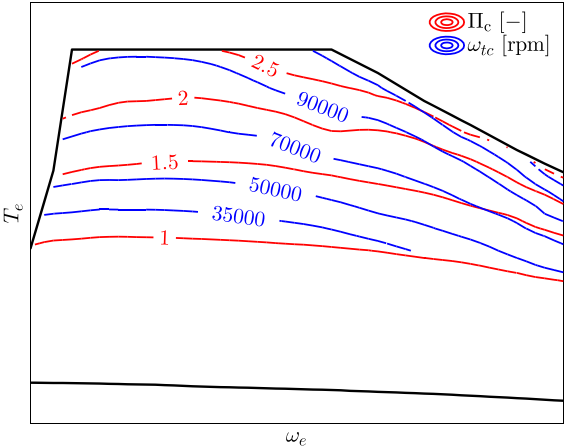


Fig. 3. Pressure ratio across the compressor and turbocharger speed under stationary conditions.

- A3: The mass flow rate at the outlet port of the compressor \dot{m}_c is the same as the mass flow rate of air entering the engine \dot{m}_{air} .
- A4: The engine operates at a constant volumetric efficiency η_v under stationary conditions.
- A5: The pressure and the temperature at the inlet port of the compressor ($p_{c,\text{in}}$, $\vartheta_{c,\text{in}}$) are at ambient conditions (p_{amb} , ϑ_{amb}).

Under assumption A1, the mass flow rate of air can be computed from the fuel mass flow rate (12) as follows:

$$\dot{m}_{air} = \lambda^* \dot{m}_f \quad (14)$$

where $\lambda^* = 14.7$ is the stoichiometric air fuel ratio. Under assumptions A2–A4, the mass flow rate of air–fuel mixture entering the engine during port fuel injection can be related to the pressure of the mixture in the intake manifold by the equation

$$\dot{m}_{air} + \dot{m}_f = \frac{1}{2} \frac{p_{im}}{R\vartheta_{im}} \eta_v V_d \frac{\omega_e}{2\pi}. \quad (15)$$

The ratio of the pressure of the intake mixture p_{im} calculated from the aforementioned equation and the ambient pressure P_{amb} is shown in Fig. 3. Under assumption A5, this ratio is the same as the pressure ratio Π_c across the compressor. The turbocharger is required only in the region where $\Pi_c > 1$. For quasi-static modeling, the mass flow through the compressor and the pressure ratio across the compressor have been used as inputs for calculating the turbocharger speed by interpolation of the compressor map. The turbocharger speed thus calculated for all the operating points has also been shown in Fig. 3. To this end, the variables, such as the mass flow rate of air, the pressure ratio in intake manifold, and the turbocharger speed, are known for all the operating points in the engine map.

G. Turbolag

Due to turbolag, the torque delivered by the engine cannot be increased beyond a limit, even if the desired torque is higher. In light of this, we have defined a term “permissible engine torque,” which is the maximum torque gain ΔT with respect to the previous time instant in a sampling time. We

TABLE I
INITIAL VEHICLE SPEED FOR DIFFERENT INITIAL GEARS IN THE
EXPERIMENTS ON THE TEST BENCH. ALL SPEEDS ARE IN
KILOMETERS PER HOUR. n_g^x REFERS TO x GEAR NUMBER

| n_g^1 | n_g^2 | n_g^3 | n_g^4 | n_g^5 | n_g^7 |
|---------|---------|---------|---------|---------|---------|
| 8 | 12 | 20 | 30 | 40 | 55 |
| 15 | 15 | 25 | 35 | 50 | 65 |
| 25 | 25 | 35 | 50 | 65 | 80 |
| | 35 | 50 | 65 | 80 | 100 |
| | | 80 | 100 | 120 | |

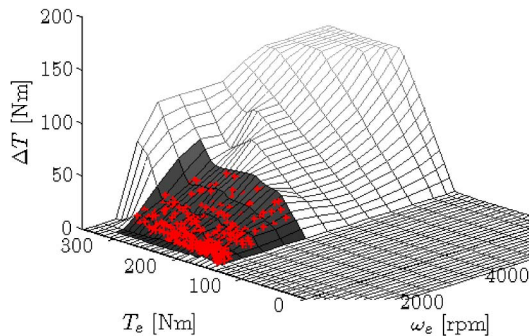


Fig. 4. Map of permissible torque obtained through regression of the experimental data. Measurements (red markers) were confined to the dark colored region; the remaining data have been extrapolated. This map is applicable only in the turbocharged region.

used experimental measurements to estimate ΔT as a function of ω_e and T_e . Numerous experiments were conducted on the test bench at full-load conditions with different initial gear n_g^{init} and initial vehicle speed v^{init} . The initial conditions of all the experiments are listed in Table I.

It is observed that the change in the engine torque in consecutive time steps is strongly correlated with the permissible engine torque. This change is calculated for all the measurements in all the experiments, and regression analysis based on the MATLAB function `scatteredInterpolant` is used to create a function map

$$\Upsilon : (\omega_e, T_e) \rightarrow \Delta T. \quad (16)$$

Thus, given the engine speed and the engine torque at the previous time step $t - 1$, the permissible torque at the current time step t can be calculated using this model. Although some experiments have different initial gear, all of them can be used together to create a single map. By initialization at different gears, it has been possible to get the data for a wide range of speed and torque. The map is actually independent of the initial gear number. The plot of the function Υ thus obtained is shown in Fig. 4.

This mapping yields a new constraint on the maximum engine torque as follows:

$$\hat{T}_{e,\max}(t) = \min \{T_e(t-1) + \Delta T, T_{e,\max}(t)\} \quad (17a)$$

$$\Delta T = \Upsilon(\omega_e(t-1), T_e(t-1)). \quad (17b)$$

Equation (17) is used only when $\Pi_c > 1$. The engine torque in the naturally aspirated region $\Pi_c < 1$ is almost instantaneously achieved within 200–300 ms. Thus, in this region, the permissible torque is set to 0, to avoid interpolation errors at

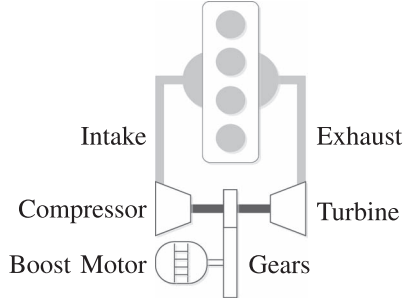


Fig. 5. Turbocharger with an electric machine coupled to its shaft.

the boundary, but this fact has been considered in the vehicle model. Most of the measurements were made at low engine speeds, i.e., less than 3000 r/min whereby the effect of turbolag is the most prominent. At speeds greater than 3000 r/min, high ΔT has been manually specified, and the engine torque is limited by $T_{e,\max}$ and not ΔT . The turbolag decreases with an increase in the engine speed. Therefore, the permissible engine torque increases. In summary, the limits on the engine torque, as a function of the engine speed, can now be defined as

$$T_{e,\min}(\omega_e(t)) \leq T_e(t) \leq \hat{T}_{e,\max}(\omega_e(t), \omega_e(t-1), T_e(t-1)). \quad (18)$$

H. Boost Mechanism

The boost motor is directly coupled to the shaft of the turbocharger, as shown in Fig. 5. The control input P_{tc} defines the electrical power demanded from the boost motor. Typically, power on the order of 5 kW is sufficient to eliminate the major turbolag [15]. Hence, P_{tc} is constrained by

$$P_{tc,\min} \leq P_{tc} \leq P_{tc,\max} \quad (19)$$

where $P_{tc,\min} = 0$ kW and $P_{tc,\max} = 5$ kW. Depending on the amount of electrical turbocharging, the limit on the engine torque imposed by the turbolag model can be increased. This mechanism for power assist is related to the energy required to accelerate the turbocharger by the dynamics equation

$$\Theta_{tc} \dot{\omega}_{tc} = \frac{P_t - P_c + \eta_{tc} P_{tc}}{\omega_{tc}}. \quad (20)$$

Here, P_t and P_c represent the power of the turbine and the compressor, respectively. Θ_{tc} is the moment of inertia of the turbocharger, η_{tc} is the efficiency of the boost mechanism accounting for the energy losses, and $\dot{\omega}_{tc}$ is the angular acceleration of the shaft of the turbocharger. Under stationary conditions, P_t and P_c can be assumed to be equal in magnitude. Thus, the simplified dynamics of the shaft takes the form

$$\Theta_{tc} \dot{\omega}_{tc} = \eta_{tc} \frac{P_{tc}}{\omega_{tc}}. \quad (21)$$

To complete the description of the boost mechanism, the dynamics of turbocharger is related to the torque constraint imposed by the turbolag (17). Recall Fig. 3, where the turbocharger speed was calculated for all the engine operating points. It is now used to calculate the turbocharger speed at

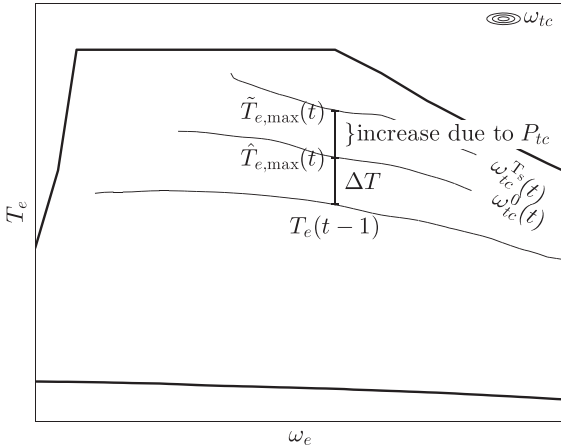


Fig. 6. Mechanism for electrical boost.

an operating point defined by $(\hat{T}_{e,\max}(t), \omega_e(t))$ at any time instant t . This would be the speed of the turbocharger if the constraint (17) is active. In other words, this speed of the turbocharger is achievable without any need of electrical turbocharging. Now, the differential equation (21) can be integrated over a sampling time for a given P_{tc} , to calculate the new turbocharger speed as follows:

$$\omega_{tc}^{T_s}(t) = \sqrt{(\omega_{tc}^0(t))^2 + 2 \eta_{tc} \frac{P_{tc} T_s}{\Theta_{tc}}} \quad (22)$$

where the initial condition is given by

$$\omega_{tc}^0(t) = \omega_{tc}|_{(\hat{T}_{e,\max}(t), \omega_e(t))}. \quad (23)$$

The new turbocharger speed $\omega_{tc}^{T_s}(t)$ defines a new limit on the maximum engine torque $\tilde{T}_{e,\max}$, which is calculated by inverting the plot of the turbocharger speed in Fig. 3. This mechanism is graphically described in Fig. 6.

Thus, the engine torque constraint (18) can now be written as

$$T_{e,\min}(\omega_e(t)) \leq T_e(t) \leq \tilde{T}_{e,\max}(t) \quad (24)$$

where

$$\tilde{T}_{e,\max}(t) = \text{fn}(\omega_e(t-1), T_e(t-1), \omega_e(t), P_{tc}(t), \omega_{tc}(t)). \quad (25)$$

I. Battery

The sum of power from the two motors and auxiliary electric power (taken as constant) is the net power input, which is also called the terminal power P_b of the battery. The terminal current I_b is defined by

$$I_b = \frac{P_b}{U_b} \quad (26)$$

$$P_b = P_m + P_{tc} + P_{aux} \quad (27)$$

where U_b is the terminal voltage. It can be expressed as a function of the open-circuit voltage U_{oc} , the terminal power P_b ,

and the internal resistance of the battery R_b as

$$U_b = \frac{U_{oc}}{2} + \sqrt{\frac{U_{oc}^2}{4} - P_b R_b}. \quad (28)$$

The terminal power is a quadratic function of the terminal voltage. By calculating the derivative of P_b with respect to U_b , the limits on the terminal power can be derived as [1]

$$P_{b,\min} \leq P_b \leq P_{b,\max}. \quad (29)$$

The state of charge (SoC) of the battery ξ , which is also one of the states in the control problem, is the ratio of charge Q and charge capacity Q_0 , i.e.,

$$\xi = \frac{Q}{Q_0}. \quad (30)$$

The SoC must lie in a SoC window, i.e., 0.2–0.8 in this case, defined by the quantity of charge that the battery can store while charging and discharging. Therefore

$$\xi_{\min} \leq \xi \leq \xi_{\max}. \quad (31)$$

The variation of the SoC depends on the terminal current as follows:

$$\dot{\xi} = -\frac{I_b}{Q_0}. \quad (32)$$

An estimation of the terminal voltage and the internal resistance as a function of ξ can be done online [29]. Here, it has been used in the form of maps. Finally, substitution of (26)–(28) into (32) yields the change in SoC.

III. PROBLEM FORMULATION

The control problems for minimizing the fuel consumption and maximizing the acceleration performance have been formulated separately. A numerical optimization method, such as dynamic programming (DP), can be used to find the global optimal solution, but it requires large computation time, and it is dependent on a driving cycle, which is not known during a real-time implementation. Nevertheless, it provides a benchmark for the comparison with other control strategies. Other very well-established solution methods include model predictive control with DP (MPC-DP) [30]–[33]; stochastic DP (S-DP) [34], [35]; Pontryagin's minimum principle (PMP) [36], [37]; ECMS and its variants adaptive ECMS (A-ECMS) [38], telemetry ECMS (T-ECMS) [39], fuzzy-tuned ECMS (F-ECMS) [23]; and convex optimization with DP (Cvx-DP) [40]. All of which can be implemented online with a simple model, achieving near-optimal results. The presence of multiple states in this system increases the computational effort in DP because of the so-called *curse of dimensionality*. At the same time, it is also cumbersome to tune the costates in PMP and ECMS in the presence of new state constraints or new cost terms [41]. In fact, due to very same reason, the current literature on PMP is mostly limited to one state or does not account for any additional cost in the Hamiltonian. Thus, DP forms the best choice as a solution method for a multiple-state system at this stage.

A. Fuel Consumption

The fuel consumption of an engine depends on the selection of operating points in a driving cycle. The task of the controller is to optimally select these set points that attain a charge-sustaining operation, while satisfying all model and driveability constraints. In addition to the constraints derived in Section II, the total electrical power available at any time is also limited.

To model the turbolag, ω_e and T_e must be included as states. Hence, the corresponding control problem can be formulated with three states, i.e., the SoC of the battery, the engine speed, and the engine torque defined by $x := [\xi, \omega_e, T_e]$; three inputs, i.e., the engine torque split, the gear number, and the power of the boost motor defined by $u := [\zeta, n_g, P_{tc}]$; and three deterministic disturbances, i.e., the speed of the vehicle, the acceleration of the vehicle, and the driving slope defined by $w := [v, a, \alpha]$, as follows:

Objective:

$$\min \left\{ \phi(\xi(T)) + \int_0^T \dot{m}_f dt \right\} \quad (33a)$$

Constraints:

$$\xi_{k+1} = \xi_k - \frac{I_b(x_k, u_k, w_k)}{Q_0} T_s \quad (33b)$$

$$T_{e,k+1} = (1 - \zeta_k) T_{gb,k}(x_k, u_k, w_k) \quad (33c)$$

$$\xi_{\min} \leq \xi_k \leq \xi_{\max} \quad (33d)$$

$$P_{b,\min}(\xi_k) \leq P_{b,k} \leq P_{b,\max}(\xi_k) \quad (33e)$$

$$\omega_{e,\min} \leq \omega_{e,k} \leq \omega_{e,\max} \quad (33f)$$

$$T_{e,\min}(\omega_{e,k}) \leq T_{e,k} \leq \tilde{T}_{e,\max} \times (\omega_{e,k-1}, T_{e,k-1}, \omega_{e,k}, P_{tc,k}, \omega_{tc,k}) \quad (33g)$$

$$\omega_{m,\min} \leq \omega_{m,k} \leq \omega_{m,\max} \quad (33h)$$

$$T_{m,\min}(\omega_{m,k}) \leq T_{m,k} \leq T_{m,\max}(\omega_{m,k}) \quad (33i)$$

$$P_{m,k} + P_{tc,k} \leq P_{el,\max} \quad (33j)$$

$$\zeta_{\min} \leq \zeta_k \leq \zeta_{\max} \quad (33k)$$

$$n_{g,\min} \leq n_{g,k} \leq n_{g,\max} \quad (33l)$$

$$P_{tc,\min} \leq P_{tc,k} \leq P_{tc,\max} \quad (33m)$$

$$\xi_0 = \xi^0, \omega_{e,0} = \omega_e^0, T_{e,0} = T_e^0 \quad (33n)$$

$$\forall k \in 0, 1, 2, \dots, N. \quad (33n)$$

The function ϕ in (33a) penalizes the end SoC, so that a charge-sustaining operation can be attained. It is a linear function given by

$$\phi(\xi(T)) = \mu_{cs} (\xi(T) - \xi^0) \quad (34)$$

where μ_{cs} is a constant, which can be derived iteratively [1]. The state dynamics (33b) and (33c) can be written explicitly in terms of the model states and inputs by substituting the model equations derived in Section II. The constraint (33j) limits the total available electrical power. The initial value of the SoC $\xi^0 = 0.6$ has been used to ensure that the battery is sufficiently charged. The initial engine speed torque ω_e^0 and T_e^0 are known by using the driving cycle. T represents the final time in the driving cycle.

B. Acceleration Performance

The objective in this case is to accelerate the vehicle as fast as possible and minimize the time required to achieve a desired speed v_{des} , starting from a given speed. In such short time spans, there is just not enough time to make the strategy charge-sustaining. Thus, it is more interesting to analyze the power split between the two motors under the constraint of fixed total available electrical power.

The control problem in this case is a minimal time problem [42], where the end time is free and must be calculated by solving the optimal control problem. However, with a slight manipulation, it can be converted into a fixed-time optimal control problem. Instead of minimizing the final time T , the final vehicle speed v_N can be maximized for a fixed time $T := NT_s$. Now, the optimal trajectory v_k^* can be used to calculate the optimal time N^* , such that $v_{N^*} = v_{des}$. For instance, the vehicle speed can be maximized at the end of 6 s, while calculating the time required to attain 100 km/h, which results in an end speed of more than 100 km/h (see Fig. 11). The time required to achieve 100 km/h can then be calculated by using interpolation.

The backward model described in Section II must be modified to solve this control problem. v and a , which were earlier known from the driving cycle, are now a part of the optimal solution. The engine torque depends on the vehicle speed and the vehicle acceleration [see (1) and (3)], which in turn define the engine speed and the limit on the maximum engine torque [see (11) and (18)]. We introduce an iterative procedure to model this recursive relationship. It is illustrated in Fig. 7.

In this approach, $T_{w,k}$ is initialized with a small value, corresponding to the maximum torque at idling speed. Then, the forward model for the vehicle dynamics (with $\alpha = 0$)

$$T_w = r_w \left((m_v + m_r)a + \frac{1}{2} \rho_{air} A_f C_d v^2 + m_v C_r g \right) \quad (35)$$

gives a unique solution for v_k and $a_k (> 0)$ using $a_k T_s = v_k - v_{k-1}$. Since v is a state, v_{k-1} is known. If this acceleration is outside the permissible limits imposed by tire slip, both v and a are corrected, and the corresponding engine speed is calculated. This speed, along with the engine speed, and the engine torque at the previous time instant define the maximum torques $\hat{T}_{e,\max}$ and $\hat{T}_{m,\max}$. To maximize the acceleration, the torque on the engine side of the gearbox is defined as

$$T_{gb,k} = \hat{T}_{e,\max} + \hat{T}_{m,\max} \quad (36)$$

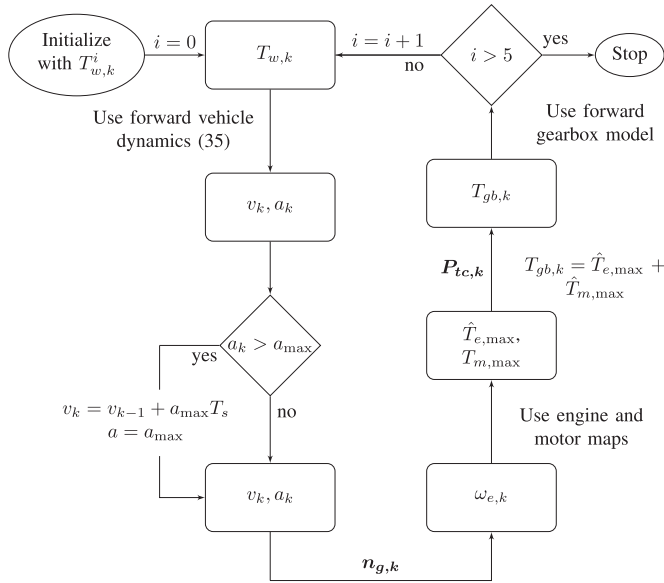


Fig. 7. Iterative procedure for model reduction. The symbols in bold represent the control inputs.

where

$$\hat{T}_{m,\max} = \min \left(T_{m,\max}, \frac{P_{el,\max} - P_{tc}}{\omega_m} \right). \quad (37)$$

Now, the torque transmitted at the wheels can be calculated by using the forward gearbox model. T_w may differ from the initialized torque. Hence, the procedure is repeated until $T_{w,k}$ and $T_{gb,k}$ are consistent, i.e.,

$$T_{gb} - \frac{T_w}{\gamma} < \epsilon. \quad (38)$$

The algorithm converges in less than five steps with $\epsilon < 0.1$. The outcome of this procedure is that the operation is always at the maximum available torque, except when the acceleration is saturated at its maximum limit. The reduced problem can be summarized with three states $x := [v, T_e, n_g]$ and two inputs $u := [n_g, P_{tc}]$ as follows:

Objective:

$$\min -v_N \quad (39a)$$

Constraints:

$$v_{k+1} = h(x_k, u_k) \quad (39b)$$

$$T_{e,k+1} = l(x_k, u_k) \quad (39c)$$

constraints (33f)–(33m)

$$a_k \leq a_{\max} \quad (39d)$$

$$v_0 = v^0, n_{g,0} = n_g^0, T_{e,0} = T_e^0$$

$$\forall k \in 0, 1, 2, \dots, N \quad (39e)$$

where h and l are nonlinear functions given by the iterative procedure.

TABLE II
DIFFERENT SCENARIOS FOR COMPARING VEHICULAR PERFORMANCE

| | Case I | Case II |
|---------------|--------------|--------------|
| ICE | Turbocharged | Turbocharged |
| $P_{e,\max}$ | 155 kW | 155 kW |
| $P_{m,\max}$ | 20 kW | 20 kW |
| $P_{tc,\max}$ | 5 kW | 0 kW |
| $P_{el,\max}$ | 20 kW | 20 kW |
| $E_{b,0}$ | 1.2 kWh | 1.2 kWh |

TABLE III
COMPARISON OF NORMALIZED FUEL CONSUMPTION [-] WITH TURBOLAG AND WITHOUT TURBOLAG CONSTRAINT IN NEDC AND WLTC. THE FINAL SOC IS THE SAME AS THE INITIAL SOC IN ALL THE SIMULATIONS

| | without lag | with lag |
|------|-------------|----------|
| NEDC | 0.999 | 1.000 |
| WLTC | 0.998 | 1.000 |

IV. OPTIMIZATION RESULTS

A. Simulation Environment

The parameters of the reference HEV described in Section II are used throughout Section IV. To analyze the effectiveness of the e-boost mechanism in an HEV, the operation strategies in two different scenarios will be compared (see Table II). Case II represents an HEV without the electrically assisted turbocharger, i.e., the boost motor is always switched off. Hence, the traction motor is the only active electric machine. In the other case, both traction motor and boost motor are active, but the maximum electrical power $P_{el,\max}$ is equal in both cases. With an additional degree of freedom, the total electrical power is optimally distributed between the two motors in Case I. All the other vehicle parameters, including vehicle mass, are the same in both cases. The scaling of motor and engine maps for the purpose of powertrain sizing will be discussed in Section V.

Sampling time of 0.1 s is used wherever not specified. The control problem was solved by using the MATLAB-based dpm function [43]. All the simulations were carried out on 2.7-GHz i7 processor. In the context of the energy management in HEVs, the approach to solve the problem by DP has been adapted from [1].

B. Fuel Consumption

An initial investigation on fuel consumption of the reference vehicle was done in common driving cycles, such as the New European Driving Cycle (NEDC) and the Worldwide harmonized Light vehicles Test Cycle (WLTC). The results are shown in Table III. The difference in fuel consumption between the models with and without turbolag constraint (17) shows that the turbolag does not affect the fuel consumption to a great extent in these cycles, which also rules out potential benefits of employing another electrical machine in the form of boost motor.

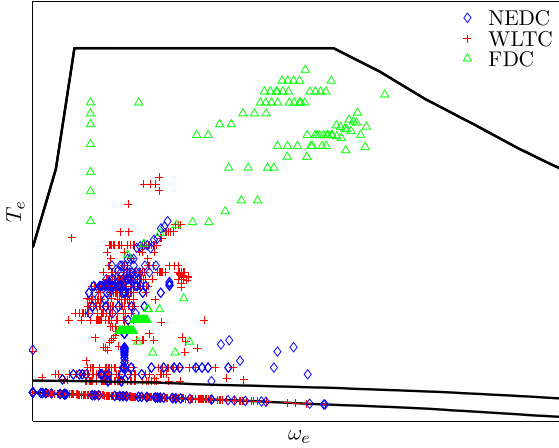


Fig. 8. Engine operating points in NEDC, WLTC, and FDC without turbolag constraint. In FDC, 25.5% of the points lie in the turbocharged region of the map, while in NEDC and WLTC, this fraction is significantly low, i.e., 0.5% and 2.3%, respectively.

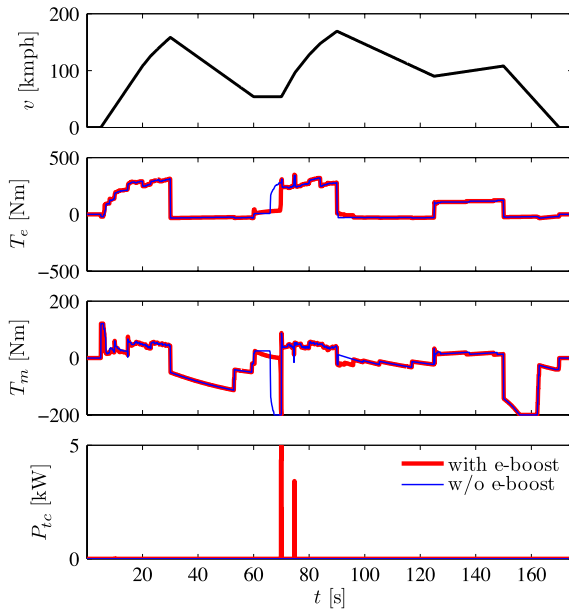


Fig. 9. Simulations for Case I (with e-boost) and Case II (w/o e-boost) in FDC with a heuristics-based gear strategy.

The operating points in NEDC and WLTC are illustrated on the engine map in Fig. 8. The plots show that the torque demands in these cycles are too low and most of the operating points lie in the naturally aspirated region of the engine map. Therefore, a new driving cycle called Fast Driving Cycle (FDC) is considered, which has more rapid acceleration phases and thus higher torque demands. This driving cycle is shown in Fig. 9.

It resembles a driving pattern in mild/heavy traffic conditions on highways. An important feature of this cycle is the frequent change in power required to drive the vehicle. In addition, the maximum acceleration in FDC is 2.4 m/s^2 , which is much higher than in NEDC and WLTC. A comparison between the two model cases defined in Table II was done by using a heuristics-based gear strategy, which is the same in both cases.

TABLE IV
COMPARISON OF NORMALIZED FUEL CONSUMPTION [-] IN CASE I
(WITH E-BOOST) WITH RESPECT TO CASE II (WITHOUT E-BOOST)
IN FDC WITH A HEURISTICS-BASED GEAR STRATEGY. THE E-BOOST
SHOWS IMPROVEMENT IN FUEL ECONOMY BY 0.7%

| | Case I | Case II |
|--------------------------------------|-----------------|-----------------|
| Fuel Consumption $\xi(T) - \xi^0$ | 0.993 -0.001 | 1.000 -0.003 |

The resulting engine torque, the traction motor torque, and the power of the boost motor are shown in Fig. 9. The main difference in the strategies arises in the events of high gradients in the torque demands. For instance, between 66 and 70 s in Case I, the boost motor assists the engine in overcoming the turbolag, while in Case II, the engine starts earlier to reduce the effect of turbolag. To compensate for a short running time and still achieve a charge-sustaining strategy, the engine in Case I produces higher torque in the later part of the driving cycle. It is observed that the fuel consumption in Case I is lower by 0.7% (see Table IV). The boost motor is used intermittently, initially for 0.3 s and later for 0.1 s.

Overall, using a boost motor in an HEV does not show major improvement in the fuel economy. However, the results suggest that it could be beneficial in special circumstances, such as in a driving cycle with frequent high torque demands during which a charge-sustaining strategy is not possible. On such occasions, instead of using the traction motor, the boost motor can be used to reduce the turbolag and still achieve high torque requirements. In this process, less electrical energy is used from the battery (but results in more fuel consumption), and it is possible to make the strategy charge-sustaining.

C. Acceleration Performance

A comparison is again made between an HEV with a boost motor (Case I) and an HEV without a boost motor (Case II). In Case II, due to turbolag, the engine torque cannot be built up fast enough, whereas in Case I, the boost motor speeds up the turbocharger and, as a result, more power is instantaneously available from the engine. This effect is illustrated in Fig. 10. For instance, at 1 s, both the engine speed and the engine torque are higher in Case I. The performance analysis is further discussed through standard test criteria.

1) *Acceleration at Full Throttle From 0 to 100 km/h:* In this criteria, the time required to accelerate from 0 to 100 km/h is calculated. The vehicle is initially at rest and is then accelerated at full throttle such that the engine speed is equal to its idling speed at launch. The optimal control inputs along with the vehicle speed are shown in Fig. 11. The main difference in the control strategies arises between 0.3 and 0.7 s. During this time, the boost motor uses 5 kW of electrical power in Case I, which leaves 15 kW for the traction motor. Hence, the traction motor torque is less in Case I during this time. The gain in the engine power due to the reduction in turbolag exceeds the loss in the traction motor power, which accelerates the vehicle faster. Beyond 0.7 s in Case I and 1.5 s in Case II, the operation is at the maximum engine torque and the

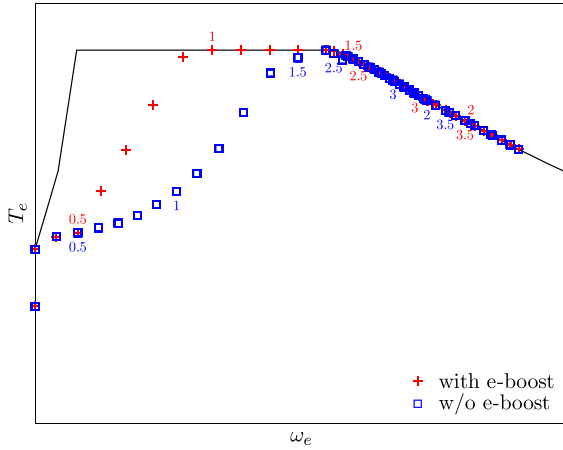


Fig. 10. Torque–speed trajectory for the two cases while accelerating from 0 to 100 km/h. Time displayed near the markers is in seconds. For the first 0.3 s, the engine rotates at the idling speed.

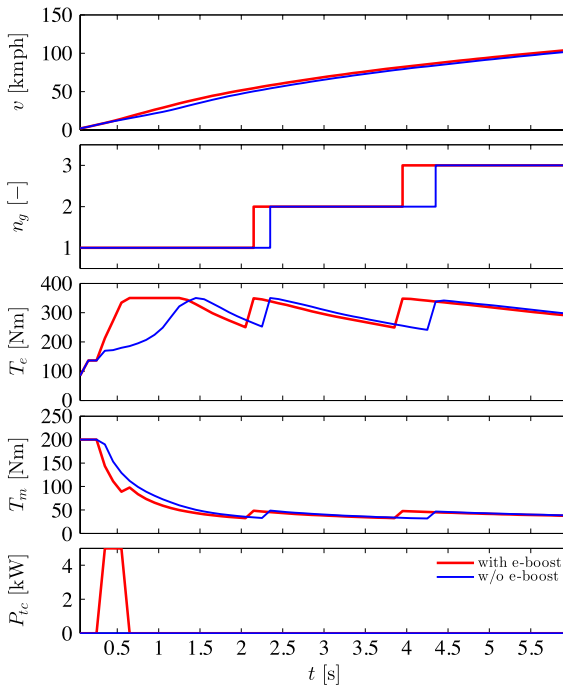


Fig. 11. Control strategy for minimizing acceleration time while accelerating from 0 to 100 km/h. At the end of 6 s, vehicle speeds in Case I (with e-boost) and Case II (w/o e-boost) are 104.19 and 101.89 km/h, respectively.

maximum engine power, respectively. Therefore, the turbolag is not observed. Gear shifts in Case I occur earlier because the same vehicle speed is achieved in less time than in Case II. It should be noted that the boost motor is used after a small delay of 0.3 s at the start because, until this time, the engine speed and the speed of the drivetrain are not synchronized and the engine continues to rotate at the idling speed. The maximum engine torque at the idling speed lies in the naturally aspirated region, and it cannot be increased further by using the boost motor.

2) *Acceleration at Full Throttle From 80 to 120 km/h in Fifth Gear:* In this criteria, the vehicle is assumed to be moving at a

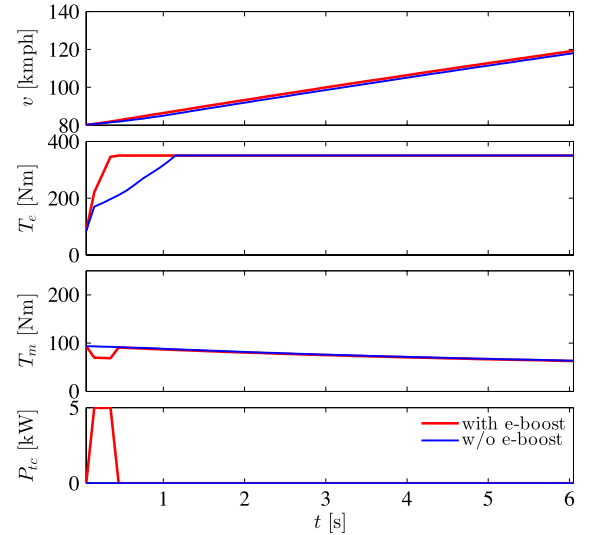


Fig. 12. Control strategy for minimizing acceleration time while accelerating from 80 to 120 km/h. At the end of 7 s, vehicle speeds in Case I (with e-boost) and in Case II (w/o e-boost) are 124.67 and 123.40 km/h, respectively.

TABLE V
ACCELERATION PERFORMANCE COMPARISON IN CASE I
(WITH E-BOOST) AND CASE II (WITHOUT E-BOOST). THE E-BOOST
OFFERS UP TO 4% REDUCTION IN ACCELERATION TIME

| | | Case I | Case II |
|----------------|---------------------------------|-------------|---------|
| 0-100 kmph | Time elapsed [s] (% reduction) | 5.54 (4%) | 5.77 |
| | Mass of fuel burnt [g] | 67.5 | 66.5 |
| | Electrical energy consumed [kJ] | 127.5 | 134.8 |
| 80-120 kmph | Time elapsed [s] (% reduction) | 6.18 (3.1%) | 6.38 |
| | Mass of fuel burnt [g] | 40.9 | 40.5 |
| | Electrical energy consumed [kJ] | 137.8 | 142.4 |

constant speed of 80 km/h and is then accelerated at full throttle constantly in the fifth gear. Therefore, only two control inputs are required to be optimized. In a higher gear, the acceleration is lower, and the vehicle needs more time to accelerate. The simulation results are shown in Fig. 12. Again, with the help of the boost motor, the time required to accelerate from 80 to 120 km/h is less in Case I. The control strategies for the two cases differ mainly between 0 and 0.5 s, when the boost motor is active. The change in behavior of the strategies in both the cases is similar to what is observed in the first test criteria, except that now the boost motor is used immediately after start because the engine launch speed is higher than the idling speed.

The results from both these test criteria are summarized in Table V. The time required to accelerate from 0 to 100 km/h and from 80 to 120 km/h is less in Case I by 0.23 s and 0.2 s, respectively. The benefits in acceleration response come at the expense of higher fuel consumption. Note that complete 20 kW of electrical power is used for the fastest performance in both the cases at each time instant, with the only difference being the distribution of this power between the two motors. The electrical energy consumed by the end of mission is less in Case I because the same end speed of 100 km/h or 120 km/h is achieved in less time. Overall, electrical boosting can be an energy-inefficient process. For instance, in the case of 0–100-km/h

acceleration test, the vehicle uses 7.3 kJ more electrical energy without e-boost and 1 g less fuel. Assuming an average fuel-to-electrical energy efficiency of 0.3, 0.56 g of fuel is required to generate 7.3 kJ of electrical energy, which still results in a fuel saving of 0.44 g.

V. POWERTRAIN SIZING

The results presented so far are specific to a set of model parameters. It was observed that the reduction in fuel consumption is not substantial and it is possible only in extreme circumstances, but the acceleration performance could be significantly improved. The extent of benefits may also depend on the relative size of the powertrain components, and the performance may be further improved with a different choice of the engine or the traction motor. Therefore, here, we investigate the influence of powertrain component sizes, particularly of the engine displacement volume, the size of the turbocharger, and the traction motor power on the control strategy in the case of acceleration performance. This will help to ascertain whether a boost motor should be used with a given combination of an engine and a traction motor.

A. Component Scaling

We considered three different engines and traction motors. In total, this gives a set of nine vehicle models. A boost motor capable of providing up to 5 kW, a battery with the energy storage capacity of 1.2 kWh, and other powertrain components are the same in all the models.

1) Internal Combustion Engine: All the three engines can provide the same maximum power of 155 kW and the same maximum torque of 350 N·m. The difference lies in the displacement volume of the engine and the size of the turbocharger. The displacement volume of the smallest engine is less than 2 l. It uses the biggest turbocharger (referred to as BTC) and takes the longest time to reach the reference torque. The biggest engine has the largest displacement volume and uses the smallest turbocharger (referred to as STC).

The engines were scaled under expert guidance and used the same measurements from the reference engine described earlier in Table I. With a smaller displacement volume, a bigger TC is needed to reach the desired maximum torque and power at higher engine speeds. This results in lower torques at lower engine speeds because the bigger TC is less efficient at lower mass flows and the needed pressure ratio cannot be achieved. The corresponding engine maps are shown in Fig. 13. In BTC, approximately 120 N·m is achieved without any turbolag, whereas in STC, 200 N·m can be achieved. The torque response of the three engines for a particular case is shown in Fig. 14. The bigger the size of the turbocharger, the larger its inertia and the more lag in achieving the reference torque.

2) Electric Motor/Generator: Three different traction motors of sizes 10, 20, and 40 kW are used for the comparison. The torque-speed characteristics of the three motors are shown in Fig. 15. Two motors with the nominal power of 20 and 40 kW were available. The map of 10-kW motor is obtained by scaling down the map of 20-kW motor by a factor of 0.5.

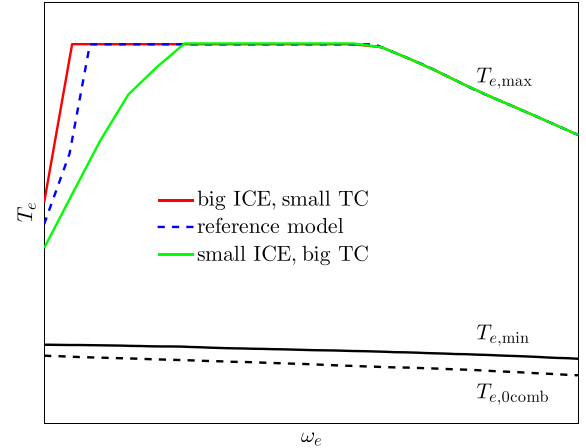


Fig. 13. Scaled engine maps with different displacement volume and size of the turbocharger. $T_{e,\min}$ and $T_{e,0\text{comb}}$ are the same in all the cases.

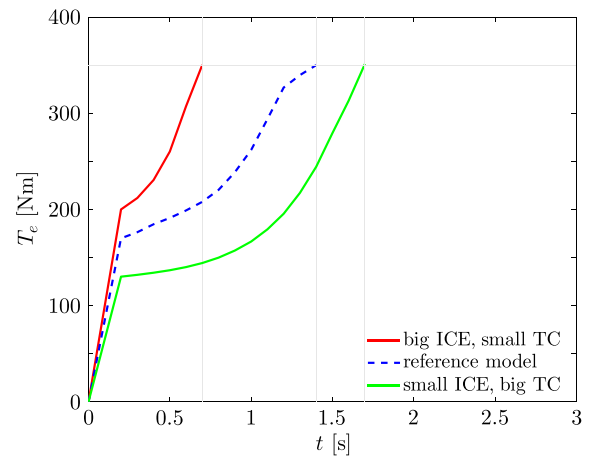


Fig. 14. Torque response of different engines at full throttle in first gear starting from 8 km/h, i.e., (n_g^1, v^8) .

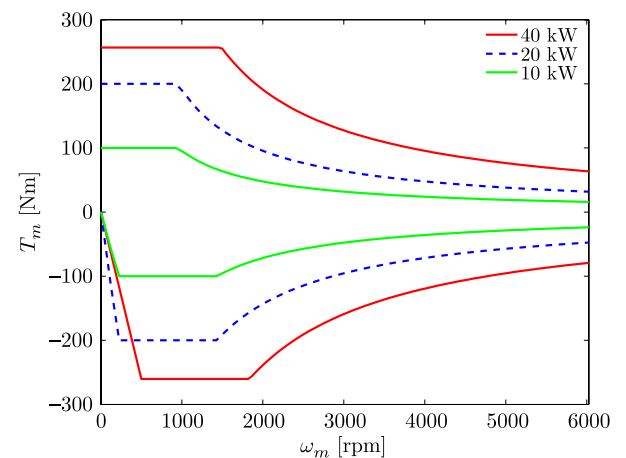


Fig. 15. Scaled motor maps with nominal power of 10, 20, and 40 kW.

B. Sizing Study

The performance of all the models is evaluated through the same tests described earlier. The influence of different sizes

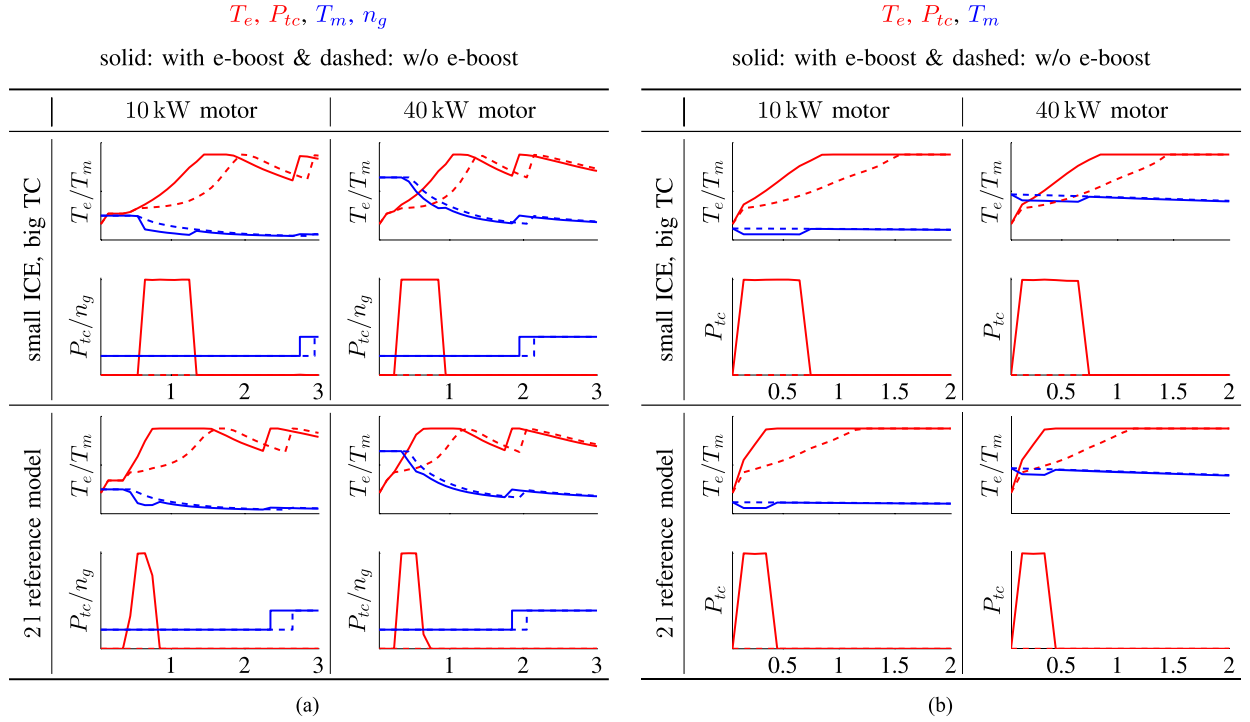


Fig. 16. Influence of the engine size and the traction motor size on the operation strategy. (a) Acceleration from 0 to 100 km/h with the optimal gear strategy (gear shift shown from 1 to 2 only). (b) Acceleration from 80 to 120 km/h in fifth gear.

of the engine and the traction motor is shown in Fig. 16. Due to space limitations, we have restricted the qualitative comparison to only four models. With any size of the engine or the motor, the acceleration performance with the e-boost is better. However, the amount of benefits vary with the size. This can also be observed from the gear up-shift pattern. The gear shift from 1 to 2 occurs earlier in Case I because the same engine speed is reached earlier [see Fig. 16(a)]. The optimal control of the electrical boost P_{tc} in most of the models results in a bang–bang solution, i.e., switching discretely between 0 and 5 kW. It lies between 0 and 5 kW only if the engine torque cannot be increased further by using more boost power, for instance, at 0.6 s in the model with the reference engine and 40-kW motor.

Specifically in the 0–100-km/h performance test with e-boost, for any combination of the engine and the motor size, it is observed that the boost motor is used after a small delay at the start, i.e., 0.2–0.5 s depending upon the model. During this time, the clutch is slipping, and the engine rotates at the idling speed. The engine delivers torque corresponding to the maximum torque at this speed, which lies in the naturally aspirated region of the engine map. Hence, the boost motor is not functional until the engine speed and the drivetrain speed are synchronized. For a fixed engine size, this delay decreases with an increase in the traction motor size. The biggest motor can deliver more torque; hence, the acceleration is more at the startup, and the speeds of the drivetrain and the engine match earlier. Due to a higher acceleration, the maximum engine torque is reached earlier, which has an influence on the duration for which the boost motor is used in the optimal strategy.

For a fixed motor size, the benefits of the boost mechanism are the most visible with the smallest engine. Because of the higher turbolag, the boost motor is used for a longer duration. This time decreases with an increase in size of the engine. Correspondingly, the time required to accelerate is not much affected by the boost mechanism in the big engine, which suffers from less turbolag.

The time T required to achieve the end speed of 100 km/h or 120 km/h for all the models is shown in Fig. 17. The maximum absolute reduction in T is seen with the smallest traction motor (10 kW). Percent reduction in T is comparable for the smallest engine with the biggest turbocharger (BTC) and the reference model (RTC) for all motor sizes, and it is much less for the biggest engine with the smallest turbocharger (STC). For a given engine, percent reduction in T decreases with an increase in size of the motor.

In principle, the boost mechanism improves the performance of HEVs, irrespective of the model size and the performance criteria. In comparison to the reference model, the magnitude of benefits is less with a relatively smaller turbocharger and more with a smaller traction motor.

VI. ROBUSTNESS ANALYSIS

To this end, a simple model of the system has been developed. It was further scaled to study the impact of the size of the traction motor and the engine. In the whole process, many assumptions were made both in modeling and in scaling. As a final step, this scaled system is tested with very low efficiency of the boost mechanism to examine the robustness of

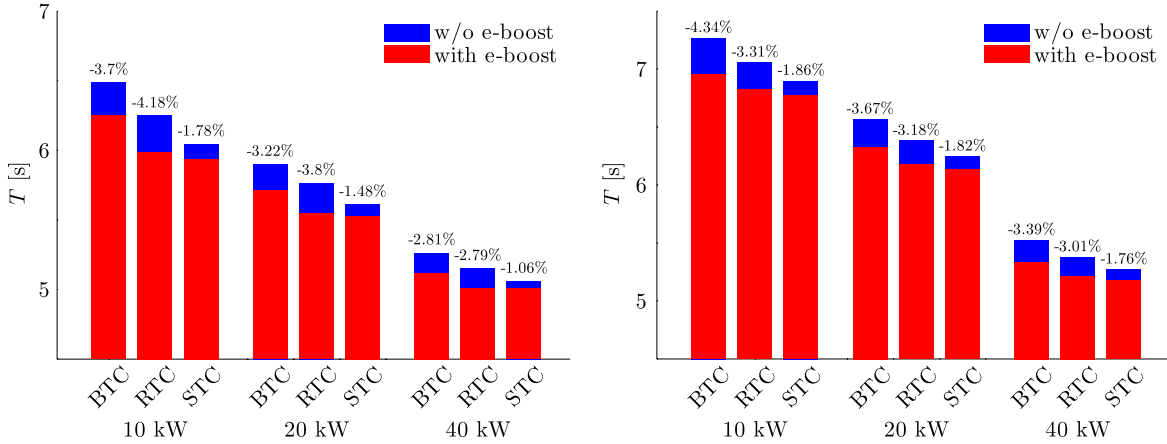


Fig. 17. Time required to accelerate (left) from 0 to 100 km/h and (right) from 80 to 120 km/h, with and without e-boost, for different models. Number over the bars shows percent reduction in time due to e-boost.

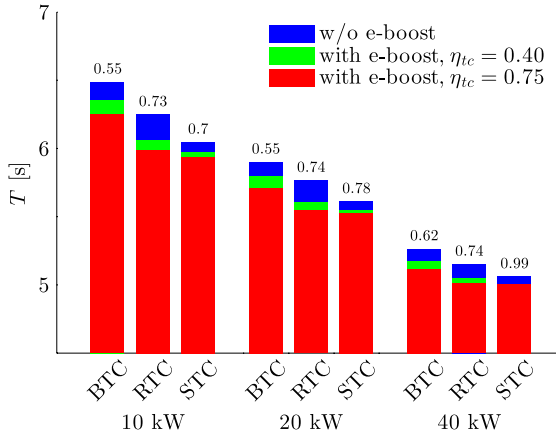


Fig. 18. Time required to accelerate from 0 to 100 km/h in Case I with high η_{tc} , Case I with low η_{tc} , and Case II (w/o e-boost) for different models. Number over the bars denotes the fraction of reduction achieved with 40% efficiency in comparison to 75% efficiency. The limiting efficiency, where the e-boost mechanism is rendered useless, is around 10%–15%.

the system. Now, η_{tc} has been chosen to be 0.4, instead of 0.75, which was used earlier. Specifically, the comparisons have been done for Case I with high η_{tc} and Case I with low η_{tc} against Case II in the 0–100-km/h performance test.

Forty percent efficiency of the boost mechanism means that, with a power demand of 5 kW, the boost motor can provide only 2 kW for reducing the turbolag. Hence, this system takes longer time to reach the maximum engine torque because less power is available at every time step. Consequently, the boost motor is used for a longer duration. The comparison of the final time is presented in Fig. 18. Evidence that the optimal strategy prefers to reduce the turbolag with the e-boost, even with such low efficiency of the boost mechanism confirms the robustness of the model despite many assumptions. The limiting efficiency of this model is found to be as low as 10%–15%.

VII. CONCLUSION

Energy management in a torque-assist HEV with an electrically assisted turbocharger has been studied. The electric ma-

chine coupled to the turbocharger is capable of accelerating it and reducing the turbolag. This approach is used to analyze the effect of turbolag on the fuel consumption and acceleration performance. A framework to model and solve the optimal control problem has been established. DP is used to solve this problem for optimizing the performance with respect to fuel consumption and acceleration performance, with the control variables being the torque split between the engine and the electric motor, the amount of electrical turbocharging, and the gear number.

Reducing the turbolag with the boost motor does not improve the fuel economy in the real-world driving cycles, mainly because the torque demands in these cycles are too low and only a few operating points lie in the turbocharged region of the engine map. Even under high torque requirements, the boost motor reduces the fuel consumption only slightly. Thus, it is not recommended to use an electrically assisted turbocharger for the sake of only fuel economy. A secondary advantage of using a boost motor is the capability to obtain a charge-sustaining strategy under high load requirements, when energy recuperation is not quite possible. Operating the boost motor in the generator mode can potentially provide fuel saving, an aspect which has not been explored in this work.

The acceleration response of this vehicle can be improved substantially by using an electrically assisted turbocharger. This has been verified through simulations in two standard test criteria, i.e., acceleration from 0 to 100 km/h with the optimal gear strategy and from 80 to 120 km/h in the fixed gear. However, the better acceleration response comes at the expense of higher fuel consumption. The usefulness of a boost motor depends on the relative size of the powertrain components. A preliminary investigation based on scaling suggests that the magnitude of benefits increases with the reduction in size of the traction motor, and decreases with the engine using a smaller turbocharger and provides the same maximum torque and power as the reference engine. Finally, the robustness of the proposed model has also been verified by varying the efficiency of the boost mechanism.

Overall, this approach to modeling and control forms an important basis for future research, and this can be easily adapted to any HEV with any size of powertrain components.

REFERENCES

- [1] L. Guzzella and A. Sciarretta, *Vehicle Propulsion Systems*, vol. 2. Berlin, Germany: Springer-Verlag, 2013.
- [2] T. Katrašnik, S. Rodman, F. Trenc, A. Hribernik, and V. Medica, "Improvement of the dynamic characteristic of an automotive engine by a turbocharger assisted by an electric motor," *J. Eng. Gas Turbines Power*, vol. 125, no. 2, pp. 590–595, Apr. 2003.
- [3] S. Chu and A. Majumdar, "Opportunities and challenges for a sustainable energy future," *Nature*, vol. 488, no. 7411, pp. 294–303, Aug. 2012.
- [4] I. Briggs *et al.*, "Waste heat recovery on a diesel-electric hybrid bus using a turbogenerator," presented at the SAE Commercial Veh. Eng. Congr., Rosemont, IL, USA, Oct. 2012, Paper CPP-01-1945.
- [5] J. Bumby, S. Crossland, and J. Carter, "Electrically assisted turbochargers: Their potential for energy recovery," in *Proc. Hybrid Veh. Conf., IET*, 2006, pp. 43–52.
- [6] U. Hopmann and M. C. Algrain, "Diesel engine electric turbo compound technology," presented at the SAE Commercial Veh. Eng. Congr., Rosemont, IL, USA, 2003, Paper CPP-01-2294.
- [7] D. Hountalas, C. Katsanos, and V. Lamaris, "Recovering energy from the diesel engine exhaust using mechanical and electrical turbocompounding," presented at the SAE Commercial Veh. Eng. Congr., Rosemont, IL, USA, 2007, Paper CPP-01-1563.
- [8] I. G. M. Thompson, "Investigations into the effects of turbocompounding," Ph.D. dissertation, Dept. Mech. Aerosp. Eng., Queen's Univ. Belfast, Belfast, U.K., 2012.
- [9] F. G. Gerke, "Diesel engine waste heat recovery utilizing electric turbo-compound technology," in *Proc. 7th DEER*, Portsmouth, NH, USA, 2001, pp. 1–5.
- [10] R. Dijkstra *et al.*, "Experimental analysis of engine exhaust waste energy recovery using power turbine technology for light duty application," *SAE Int. J. Engines*, vol. 5, no. 4, pp. 1729–1739, 2012.
- [11] Y. Ismail, D. Durrieu, P. Menegazzi, P. Chesse, and D. Chalet, "Potential of exhaust heat recovery by turbocompounding," presented at the SAE Commercial Veh. Eng. Congr., Rosemont, IL, USA, 2012, Paper CPP-01-1603.
- [12] I. Arsie, A. Cricchio, C. Pianese, M. De Cesare, and W. Nesci, "A comprehensive powertrain model to evaluate the benefits of electric turbo compound (ETC) in reducing CO₂ emissions from small diesel passenger cars," presented at the SAE Commercial Veh. Eng. Congr., Rosemont, IL, USA, 2014, Paper CPP-01-1650.
- [13] F. Tian, G. F. Ren, B. Yan, G. Q. Ao, and L. Yang, "Optimization of hybrid turbocharger applied on common rail diesel engine with exhaust gas recirculation," *Appl. Mech. Mater.*, vol. 246/247, pp. 84–88, Dec. 2012.
- [14] P. S. Divekar, B. Aylew, and R. Prucka, "Coordinated electric supercharging and turbo-generation for a diesel engine," presented at the SAE Commercial Veh. Eng. Congr., Rosemont, IL, USA, 2010, Paper CPP-01-1228.
- [15] F. Millo, F. Mallamo, E. Pautasso, and G. G. Mego, "The potential of electric exhaust gas turbocharging for HD diesel engines," presented at the SAE Commercial Veh. Eng. Congr., Rosemont, IL, USA, 2006, Paper CPP-01-0437.
- [16] P. Pallotti, E. Torella, J. New, M. Criddle, and J. Brown, "Application of an electric boosting system to a small, four-cylinder S.I. engine," presented at the SAE Commercial Veh. Eng. Congr., Rosemont, IL, USA, 2003, Paper CPP-32-0039.
- [17] A. Sciarretta and L. Guzzella, "Control of hybrid electric vehicles," *IEEE Control Syst.*, vol. 27, no. 2, pp. 60–70, Apr. 2007.
- [18] T. E. Darlington and A. A. Frank, "Exhaust gas driven generator with altitude compensation for battery dominant hybrid electric vehicles," in *Proc. ASME Int. Combustion Engine Div. Fall Tech. Conf.*, Long Beach, CA, USA, 2004, pp. 1–10.
- [19] S. M. Shahed, "An analysis of assisted turbocharging with light hybrid powertrain," presented at the SAE Commercial Veh. Eng. Congr., Rosemont, IL, USA, 2006, Paper CPP-01-0019.
- [20] P. Tona, S. Venturi, and R. Tilagone, "Integrated powertrain control for a mild-hybrid urban vehicle with a downsized turbo-charged CNG engine," presented at the SAE Commercial Veh. Eng. Congr., Rosemont, IL, USA, 2008, Paper CPP-01-0081.
- [21] D. Boland, H.-J. Berner, and M. Bargende, "Optimization of a CNG driven SI engine within a parallel hybrid power train by using EGR and an oversized turbocharger with active-WG control," presented at the SAE Commercial Veh. Eng. Congr., Rosemont, IL, USA, 2010, Paper CPP-01-0820.
- [22] I. Kolmanovsky and A. G. Stefanopoulou, "Evaluation of turbocharger power assist system using optimal control techniques," presented at the SAE Commercial Veh. Eng. Congr., Rosemont, IL, USA, 2000, Paper CPP-01-0519.
- [23] D. Zhao, R. Stobart, G. Dong, and E. Winward, "Real-time energy management for diesel heavy duty hybrid electric vehicles," *IEEE Trans. Control Syst. Technol.*, vol. 23, no. 3, pp. 829–841, May 2015.
- [24] "Pu 106a Hybrid," Mercedes AMG Petronas Formula (M. A. P. F.) One Team, Brackley, U.K., Nov. 2014. [Online]. Available: <http://www.mercedesamg1.com/en/news/2014/2014-tech-guide-power-unit-terminologies/>
- [25] M. Kang, H. Kim, and D. Kum, "Systematic configuration selection methodology of power-split hybrid electric vehicles with a single planetary gear," presented at the ASME Dynamic Syst. Contr. Conf., San Antonio, TX, USA, 2014, Paper DS-CC-5848.
- [26] L. Eriksson *et al.*, "Modeling of a turbocharged SI engine," *Annu. Rev. Control*, vol. 26, no. 1, pp. 129–137, 2002.
- [27] I. Kolmanovsky, P. Morall, M. Van Nieuwstadt, and A. Stefanopoulou, "Issues in modeling and control of intake flow in variable geometry turbocharged engines," in *Chapman and Hall CRC Research Notes in Mathematics*. Boca Raton, FL, USA: CRC, 1999, pp. 436–445.
- [28] R. Sharma, D. Nesic, and C. Manzie, "Control oriented modeling of turbocharged spark ignition engine," presented at the SAE Commercial Veh. Eng. Congr., Rosemont, IL, USA, 2009, Paper CPP-01-0684.
- [29] H. He, X. Zhang, R. Xiong, Y. Xu, and H. Guo, "Online model-based estimation of state-of-charge and open-circuit voltage of lithium-ion batteries in electric vehicles," *Energy*, vol. 39, no. 1, pp. 310–318, Mar. 2012.
- [30] M. Back, "Prädiktive Antriebsregelung Zum Energieoptimalen Betrieb Von Hybridfahrzeugen," Karlsruhe Inst. Technol., Karlsruhe, Germany, 2005.
- [31] H. Borhan *et al.*, "MPC-based energy management of a power-split hybrid electric vehicle," *IEEE Trans. Control Syst. Technol.*, vol. 20, no. 3, pp. 593–603, May 2012.
- [32] S. Di Cairano, W. Liang, I. V. Kolmanovsky, M. L. Kuang, and A. M. Phillips, "Power smoothing energy management and its application to a series hybrid powertrain," *IEEE Trans. Control Syst. Technol.*, vol. 21, no. 6, pp. 2091–2103, Nov. 2013.
- [33] M. Koot *et al.*, "Energy management strategies for vehicular electric power systems," *IEEE Trans. Veh. Technol.*, vol. 54, no. 3, pp. 771–782, May 2005.
- [34] L. Johannesson, M. Asbogard, and B. Egardt, "Assessing the potential of predictive control for hybrid vehicle powertrains using stochastic dynamic programming," *IEEE Trans. Intell. Transp. Syst.*, vol. 8, no. 1, pp. 71–83, Sep. 2007.
- [35] C.-C. Lin, H. Peng, and J. Grizzle, "A stochastic control strategy for hybrid electric vehicles," in *Proc. IEEE Amer. Control Conf.*, 2004, vol. 5, pp. 4710–4715.
- [36] S. Delprat, J. Lauber, T.-M. Guerra, and J. Rimaux, "Control of a parallel hybrid powertrain: Optimal control," *IEEE Trans. Veh. Technol.*, vol. 53, no. 3, pp. 872–881, May 2004.
- [37] N. Kim, S. Cha, and H. Peng, "Optimal control of hybrid electric vehicles based on Pontryagin's minimum principle," *IEEE Trans. Control Syst. Technol.*, vol. 19, no. 5, pp. 1279–1287, Sep. 2011.
- [38] C. Musardo, G. Rizzoni, Y. Guezennec, and B. Staccia, "A-ECMS: An adaptive algorithm for hybrid electric vehicle energy management," *Eur. J. Control*, vol. 11, no. 4, pp. 509–524, Dec. 2005.
- [39] A. Sciarretta, L. Guzzella, and M. Back, "A real-time optimal control strategy for parallel hybrid vehicles with on-board estimation of the control parameters," in *Proc. IFAC Symp. Adv. Automot. Control*, 2004, pp. 19–23.
- [40] T. Niuesch, P. Elbert, M. Flankl, C. Onder, and L. Guzzella, "Convex optimization for the energy management of hybrid electric vehicles considering engine start and gearshift costs," *Energies*, vol. 7, no. 2, pp. 834–856, 2014.
- [41] L. Serrao *et al.*, "Open issues in supervisory control of hybrid electric vehicles: A unified approach using optimal control methods," *Oil Gas Sci. Technol.—Revue d'IFP Energies Nouvelles*, vol. 68, no. 1, pp. 23–33, 2013.
- [42] D. P. Bertsekas, D. P. Bertsekas, D. P. Bertsekas, and D. P. Bertsekas, *Dynamic Programming and Optimal Control*, vol. 1. Belmont, MA, USA: Athena Scientific, 1995.
- [43] O. Sundstrom and L. Guzzella, "A generic dynamic programming MATLAB function," in *Proc. IEEE CCA ISIC*, 2009, pp. 1625–1630.



Achin Jain received the B.Tech. degree in mechanical engineering from the Indian Institute of Technology Delhi, New Delhi, India, in 2012 and the M.Sc. degree in robotics, systems, and controls from the Swiss Federal Institute of Technology in Zurich (ETH Zurich), Zurich, Switzerland, in 2015. He is currently working toward the Ph.D. degree with the University of Pennsylvania, Philadelphia, PA, USA.

He was a Master Thesis Student with Daimler AG, Stuttgart, Germany. His research interests include controls and optimization.



Tobias Nueesch was born in Altsttten SG, Switzerland, in 1985. He received the M.Sc. degree in mechanical engineering and the Dr.Sc. degree in control engineering from the Swiss Federal Institute of Technology in Zurich (ETH Zurich), Zurich, Switzerland, in 2010 and 2014, respectively.

He is currently with the Development Department of ThyssenKrupp Presta AG, Eschen, Liechtenstein.



Pedro Macri Lassus received the Diploma degree in mechanical engineering from the University of Karlsruhe, Karlsruhe, Germany in 2005.

He is currently a Development Engineer with the Research and Advanced Engineering Powertrain Division, Daimler AG, Stuttgart, Germany.



Christian Naegele received the Diploma degree in mechanical engineering from the University of Stuttgart, Stuttgart, Germany, in 2012. He is working toward the Ph.D. degree with Brandenburg University of Technology Cottbus-Senftenberg, Cottbus, Germany.

He is currently with the Research and Advanced Engineering Powertrain Division, Daimler AG, Stuttgart.



Christopher H. Onder received the Diploma and the Ph.D. degree in mechanical engineering from the Swiss Federal Institute of Technology in Zurich (ETH Zurich), Zurich, Switzerland.

He is currently a Professor with the Institute for Dynamic Systems and Controls, ETH Zurich. He is the author and coauthor of numerous articles and a book on modeling and control of engine systems.

Dr. Onder received the BMW Scientific Award, the ETH Medal, the Vincent Bendix Award, the Crompton Lanchester Medal, and the Arch

T. Colwell Award.